Orion Orbit Control Design and Analysis

Mark Jackson[1]
Charles Stark Draper Laboratory, Houston, TX, 77058

Rodolfo Gonzalez[2]
NASA Johnson Space Center, Houston, TX, 77058

and

Christopher Sims[3]
Lockheed Martin, Houston, TX, 77058

The analysis of candidate thruster configurations for the Crew Exploration Vehicle (CEV) is presented. Six candidate configurations were considered for the prime contractor baseline design. The analysis included analytical assessments of control authority, control precision, efficiency and robustness, as well as simulation assessments of control performance. The principles used in the analytic assessments of controllability, robustness and fuel performance are covered and results provided for the configurations assessed. Simulation analysis was conducted using a pulse width modulated, 6 DOF reaction system control law with a simplex-based thruster selection algorithm. Control laws were automatically derived from hardware configuration parameters including thruster locations, directions, magnitude and specific impulse, as well as vehicle mass properties. This parameterized controller allowed rapid assessment of multiple candidate layouts. Simulation results are presented for final phase rendezvous and docking, as well as low lunar orbit attitude hold. Finally, on-going analysis to consider alternate Service Module designs and to assess the pilot-ability of the baseline design are discussed to provide a status of orbit control design work to date.

Nomenclature

I. Introduction

NASA's Crew Exploration Vehicle (CEV) is tasked with transporting astronauts to and from the International Space Station (ISS), and to and from low Lunar orbit. Both of these missions will rely on reaction control system (RCS) thrusters attached to the Service Module (SM) for attitude control, small trajectory corrections, and relative trajectory control during proximity operation and docking – both to ISS and the Lunar Surface Access Module (LSAM). The CEV Service Module differs from its Apollo predecessor in three ways that drive the RCS design. First, the CEV service module will be lighter than its Apollo counter part in order to accommodate launch vehicle performance. Smaller SM mass and rotational inertias have implications on thruster sizes required to achieve authority and precision requirements. Second, the CEV will be required to operate for months in low lunar orbit. This means that long term propellant usage is a major driver for RCS sizing and layout. Finally, the CEV SM will use solar arrays as a power source rather than the fuel cells used in the Apollo program. The size, location and orientation of SM arrays drives thruster placement, since thrust plumes are a major concern for solar array loading and heat limits.

This paper describes the analysis completed to assess and compare several candidate RCS designs for the CEV SM. A description of the candidate configurations is covered first, followed by a description of analytical assessment tools, and simulation assessment methods. The simulation section presents a control scheme that can be reconfigured for any controllable RCS configuration given system mass properties and RCS thruster locations and thrust information. Results are presented that were used to generate an RCS baseline configuration for the SM.

[1] Insert Job Title, Department Name, Address/Mail Stop, and AIAA Member Grade for first author.
[2] Insert Job Title, Department Name, Address/Mail Stop, and AIAA Member Grade for second author.
[3] Insert Job Title, Department Name, Address/Mail Stop, and AIAA Member Grade for third author.

II. RCS Trade Space and Metrics

The purpose of this CEV analysis was to canvas the trade space of potential RCS configurations and find a solution that meets requirements with good performance. RCS attributes that were trades included thruster size, thruster minimum on time, and thruster layout. Three candidate thruster sizes were considered, 100 lb, 25 lb and 14 lb. Two minimum on times were considered, 80 ms and 20 ms. Together with thrust magnitude, the minimum on time determines how precisely the controller can change the vehicle angular rate.

Thruster layout possibilities were narrowed by defining three thruster pod configurations. Candidate layouts were then defined by the pod configurations and pod locations. All options used 4 pods. Descriptions of the final candidate configurations are provided below.

The metrics, or areas assessed for each configuration were control authority, control precision, efficiency, robustness, proximity operations performance, and solar array plume impingement. RCS Control authority requirements are primarily driven by six degree of freedom control during proximity operations and docking. This may be manifested by executing translational velocity changes while maintaining attitude control, or by closed loop control around a commanded target-relative position/velocity channel. When considering translational control authority, it is important to assess both instantaneous authority, and average authority. Instantaneous authority measures the ability of the RCS to accelerate in any direction without regard for rotation, while average authority includes the effects of thruster modulation required to prevent rotation while translating. For the CEV vehicle, and the configurations assessed, rotational control authority was well above requirements, so thruster sizing was driven more by translational authority requirements.

Control precision measures the minimum rate change that can be executed in rotation or translation. Control precision requirements are driven by precise docking control, as well as attitude control fuel efficiency (the relationship between control precision and attitude control efficiency is explained below). Control precision is primarily a function of thruster size and minimum firing time, although RCS layout also plays a role – as it does for control authority.

RCS efficiency has two facets. The first type of efficiency measures the propellant used to generate acceleration in any commanded direction. In general the acceleration command is a six dimensional vector whose components include rotation and translation. This type of efficiency is primarily a function of thruster layout, since the specific impulse of thrusters in the range of sizes considered is nearly equivalent. This first type of efficiency determines how cheaply the RCS can execute maneuvers or counter disturbances.

The second type of efficiency is associated with control precision as mentioned above. Control precision determines how accurately rate changes can be executed, which in turn determines the amplitude of limit cycles during position or attitude hold. Higher rate limit cycles require more fuel, as described below.

In RCS systems, robustness may be thought of as the capability to actuate commands in the presence of thruster failures. Robustness is a function of thruster layout, since the thruster arrangement determines whether the remaining thrust vectors form a basis in the control space. Efficiency is also an important factor in robustness, since an RCS layout may require excessive fuel to actuate some commands after a thruster failure.

Although analytical techniques can provide metrics for all the criteria listed above, it is important to test candidate RCS configurations in simulation using scenarios that exercise the above attributes and provide data on the system's performance during mission critical operations. For this reason, a control law was implemented in the NASA CEV simulation which was parameterized by vehicle mass properties and thruster location, direction and magnitude. The control law was used, along with a generic RCS model, to test each configuration in the critical proximity operations and docking phase, as well as in long duration attitude hold, where fuel usage rates are paramount to Lunar outpost mission success.

The final assessment criterion was RCS plume impingement. The CEV design relies on two large solar array appendages which are extremely sensitive to the heat, pressure and contamination associated with thruster plumes. This consideration drove thruster placement and orientation as described below.

III.

IV. Candidate Configurations

A. Coordinate System

Figure 1 illustrates the body coordinate system used throughout this paper. The origin is at the combined center of mass of the Service Module

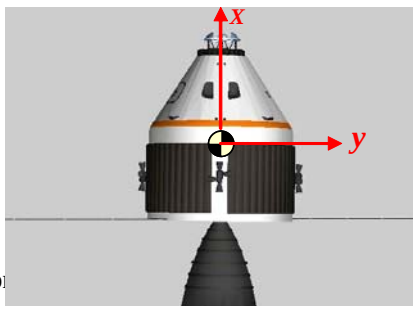

Figure 1. CEV Body Coordinate System

(SM) and the Crew Module (CM). The X axis is aligned with the longitudinal axis of the vehicle and is positive toward the "nose." The Y axis points out the right side of the vehicle, and the Z axis completes the right handed coordinate system, and points "down," away from the windows on the CM and into the page in the figure.

B. Apollo Configuration

For reference, the Apollo configuration is described. This configuration was the basis for the baseline, and modified baseline configurations described below. Figure 2 is a notional diagram of an Apollo thruster pod. Four thrusters were arranged with two facing fore-and-aft (axial thrusters) and two facing in the lateral direction (lateral thrusters). These were mounted around the Apollo service module, near the center of mass of the combined service module/command module (refer again to Figure 1 which illustrates an Apollo-like layout). This configuration provided a straightforward thruster selection map to actuate pure axis commands (Figure 3). With 100 lb thrusters, the configuration also provided good control authority and some robustness to thruster failures. When fired at a minimum on time of 20 ms, control precision was acceptable for docking with Apollo vehicle mass and inertia.

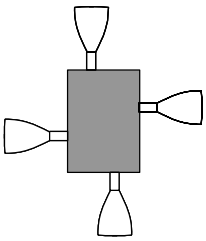

Figure 2. Apollo Thruster Pod

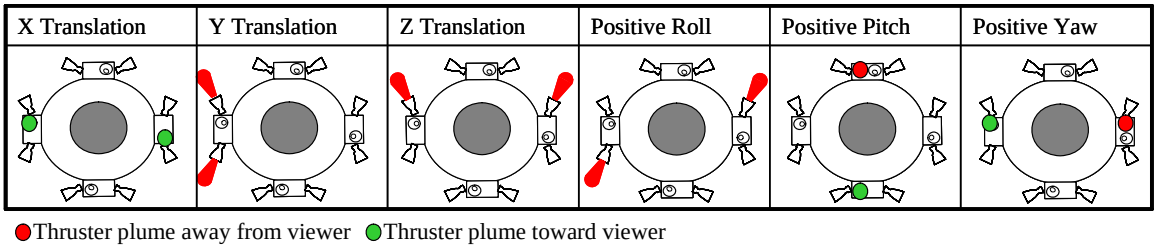

Figure 3. Apollo Thruster Selection by Axis (View from Aft)

C. Baseline and Modified Baseline Thruster Layouts

Prior to this study, a baseline thruster layout was established based on the Apollo configuration described above. In order to improve axial control authority, two additional thrusters were added in the fore and aft directions as shown in Figure 4. The pods were arranged in the same manner as the Apollo configuration, and thruster selection was also similar – except that the additional thrusters could be used when more control authority was needed for some commands. This configuration was used for preliminary sizing and fuel consumption analysis. However the configuration caused an unacceptable level of plume impingement on the CEV solar arrays.

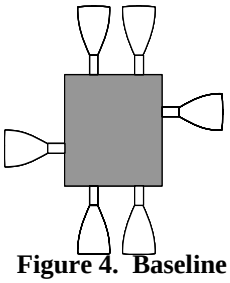

Figure 4. Baseline Thruster Pod

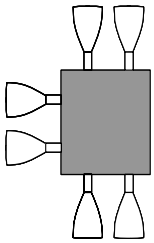

Figure 5. Modified Baseline Thruster Pod

To improve plume impingement characteristics, a modified baseline configuration was created (Figure 5). In this configuration, both of the lateral thrusters were mounted on the same side of the pod. The pods were then mounted as shown in Figure 6 (the figure shows the view from aft of the SM). The thruster pods were moved to a "narrow X" configuration with pods at 1 O'clock, 5 O'clock, 7 O'clock and 11 O'clock. This arrangement, together with the modified pod configuration resulted in reduced impingement on the arrays. This figure also shows the thruster selection for pure axis commands.

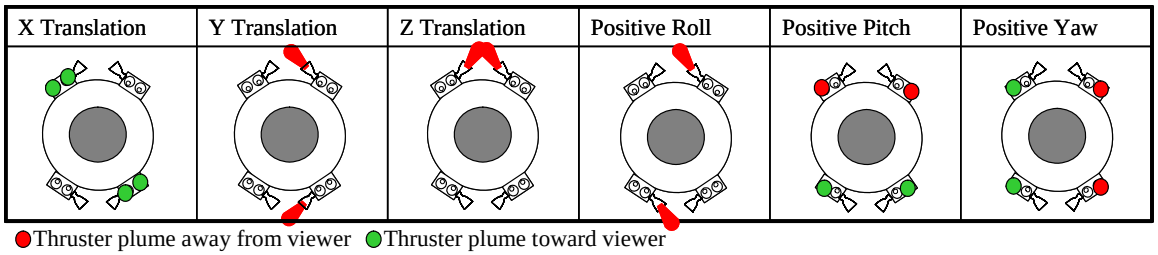

Figure 6. Modified Baseline Thruster Selection (View from Aft)

D. Block Swap Geometry (BSG) Thruster Layout

The other thruster layout analyzed was termed the Block Swap Geometry (BSG) – so named because thruster failures could be addressed simply by switching between three, nearly identical strings, or "blocks" of thrusters. Figure 7 illustrates the geometry of the Block Swap arrangement, as well as its relative, the Modified Block Swap Geometry. In either case, the orientation of thrusters with respect to an axis system attached to the pod, may be visualized by applying two sequential rotations. Starting with the exhaust vector aligned with the jet pod *x* direction (also the CEV x_{body} direction), the vector is rotated about the jet pod *z* axis by the "cant" angle thus raising the exhaust vector from the vehicle skin. Next, a second rotation (skew) is applied about the jet pod *x* axis, which has the effect of rotating the thrust vector about the CEV longitudinal axis. For regular block swap geometry, the aft-firing jet skews in the same direction as the forward-firing jet. For modified block swap, the aft-firing jet skews in the opposite direction. All configurations considered used the Modified Block Swap Geometry (MBSG) since it had better plume impingement characteristics.

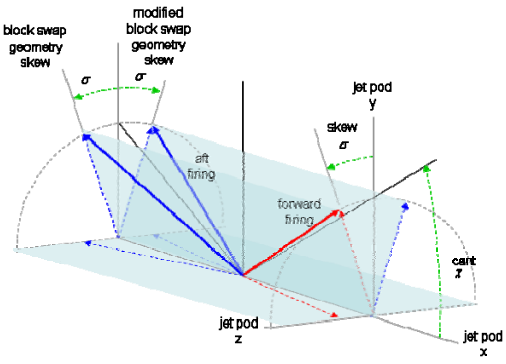

Figure 7. Block Swap Geometry Visualization

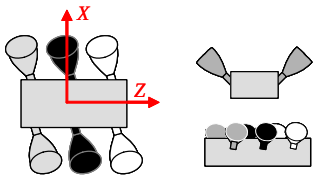

Figure 8. MBSG Pod

An example of an MBSG pod is shown in Figure 8 from top and side views, and a notional mounting scheme is shown in Figure 9. Note that since the grey, black and white thrusters are identically oriented, and nearly co-located, they produce approximately the same force and torque. Therefore the white thursters in all pods may be viewed as one string, or block, and similarly for the black and grey. So reconfiguration after a failure may be accomplished by swapping to a new string. Further, no identification of a particular failed thruster within a strung is required. Figure 9 also shows the effect of the skew angle. The green arrows in the figure represent the lateral component of the thrust vectors of the central aft firing thruster from each of the indicated pods, while the red dashed arrows indicate thrust from the corresponding forward firing thrusters. When this combination is fired as shown, a roll torque is generated due to the skew angle. This torque is small compared control torques in other axes, but this is mitigated somewhat by smaller roll inertias. Figure 10 shows the thruster selections for pure axis commands using MBSG.

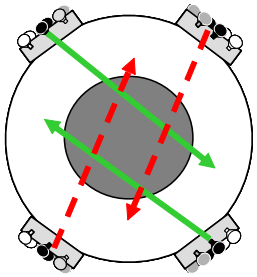

Figure 9. MBSG Pod Mounting and Effect of Skew

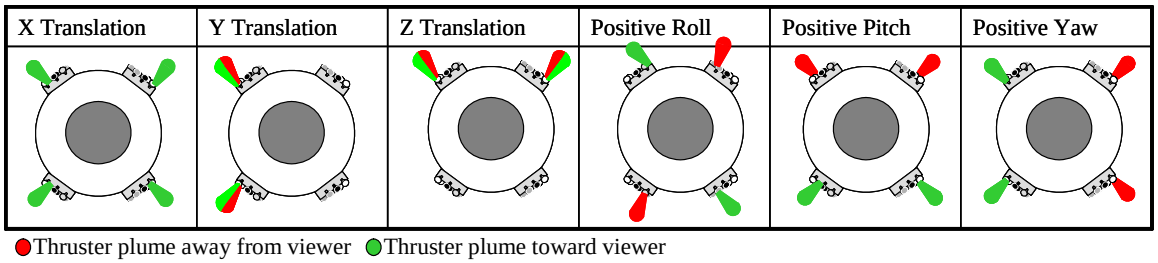

Figure 10. Modified Block Swap Geometry Thruster Selection

E. Configuration Summary

Table 1 summarizes the attributes of the six candidate configurations plus the baseline (Configuration 0). Configurations 1 and 2 used 100 lb thrusters, while 3, and 6 used 25 lb, and configurations 4 and 5 used 14 lb. For the lower thrust RCS systems (configurations 3 through 6), additional augmentation thrusters were added on the aft ring of the service module facing aft. These provided the vehicle with a backup to the main engine for critical burns, as well as an intermediate thrust level for rendezvous burns whose magnitude was too small for the main engine, but too large for efficient execution by RCS. Minimum on times were driven by control precision, but limited by thruster life considerations. In particular, it was desirable from a control point of view to fire the 100 lbf thrusters for as little as 20 ms to meet docking accuracy requirements. However, concerns about residual buildup limited the minimum on times to 80 ms for all other operations.

Table 1. Candidate RCS Configuration Summary

Attribute	Baseline (Config 0)	Config 1	Config 2	Config 3	Config 4	Config 5	Config 6
Thrust	100 lbf	100 lbf	100 lbf	25 lbf	14 lbf	14 lbf	25 lbf
Number of pods	4	4	4	4	4	4	4
Thrusters per pod	6	6	6	6	6	6	6
Thruster orientation	Baseline	Modified Baseline	Modified Block Swap	Modified Baseline	Modified Block Swap	Modified Block Swap	Modified Block Swap
Pod Location	SM middle	SM Aft	SM Forward	SM Forward	SM Forward	SM Aft	SM Aft
Thruster Cant	15 deg	15 deg	15 deg	45 deg*	45 deg	45 deg	45 deg
Thruster Skew	NA	NA	8 deg	NA	8 deg	8 deg	8deg
Augmentation Engines	No	No	No	4, 870 lbf	6, 240 lbf	8, 125 lbf	8, 125 lbf
Minimum Impluse for Proximity Operations	20 ms	20 ms	80 ms	80 ms	80 ms	80 ms	80 ms
Mimimum Impulse for Attitude Hold	80 ms	80 ms	80 ms	80 ms	80 ms	80 ms	80 ms

* Lateral thrusters in this configuration are canted at 15 degrees, axial thrusters at 45 degrees

Figure 11 provides a visualization of configurations 1 through 6. The red line segments represent the thruster exhaust directions, and their length is proportional to thrust magnitude. The figures do not include any of the augmentation thrusters.

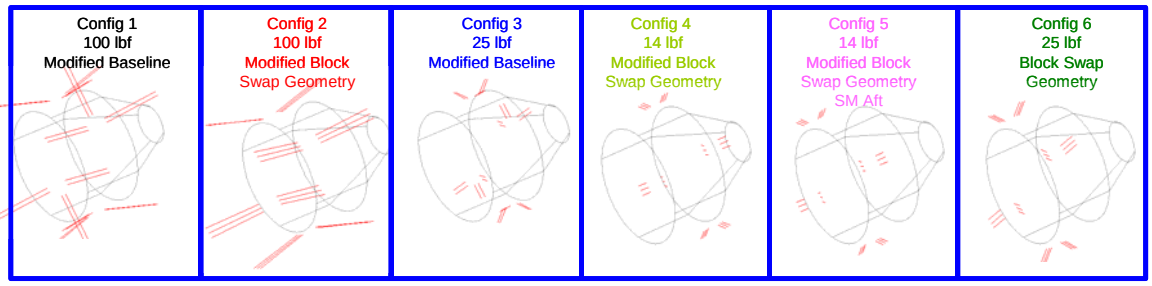

Figure 11. Visualization of RCS Configurations

V. Off-line Assessment

This section describes the tools and techniques used in the off-line assessment of the candidate configurations.

F. Simplex Thruster Selection

A simplex thruster selection algorithm was used for many of the assessments described below, so some background on the algorithm is provided here, with references for interested readers.

The generic simplex algorithm (Ref. [SIMPLEX]) minimizes a scalar cost function, $J=c^T x$, where x is a vector of control variables and c is a weighting vector whose elements represent the costs of each control. J is minimized subject to the constraints, $Ax=b$, and all $x \geq 0$. For the thruster selection problem, the elements of x are commanded on-times for each thruster, while the elements of c are usually the fuel flow rate for each thruster. This means that J is the amount of fuel used to fire the thrusters for x_i seconds each.

The constraint, $Ax=b$, expresses the fact that the on-time vector x must actuate a command. Here, A is a matrix whose columns are the accelerations – rotational and/or translational – achieved by each thruster, and b is a commanded angular and/or translational velocity change. Obviously all elements of x must be greater than zero, since negative on-times are not allowed. The dimensions of A and b depend on the degrees of freedom to be controlled. In this context, we usually either control three translational degrees, three rotational degrees, or both simultaneously.

For the purposes of this study, the simplex algorithm was used as part of an off line tool suite, as well as the thruster selection algorithm in a 6 DOF simulation. As a component of a real-world control system, the algorithm is well suited for some applications, and less so for others. However, for RCS configuration analysis, simplex allows rapid reconfiguration of tools and simulations for assessment of multiple candidates.

G. Authority and Precision

Instantaneous control authority was assessed by creating a thruster table for single axis commands, and determining the translation and rotation control accelerations in each axis and comparing them to requirements. This type of authority provided a measure of responsiveness to input commands from the crew or from automated guidance algorithms. The generation of single axis thruster tables also helped to provide insight into how each configuration actuates commands.

To assess average control authority, a simplex algorithm was used to calculate the time and propellant required to achieve rotational and translational rate changes of 1°/s and 1 ft/s. Average acceleration is the rate change command, divided by the longest thruster on time - max(x). Since the RCS configurations typically provided rotational thruster combinations that produced virtually no translation, the primary concern for average authority was in translation. Putting the simplex algorithm in a loop allowed a search for the worst average acceleration through all translation directions with zero rotation command.

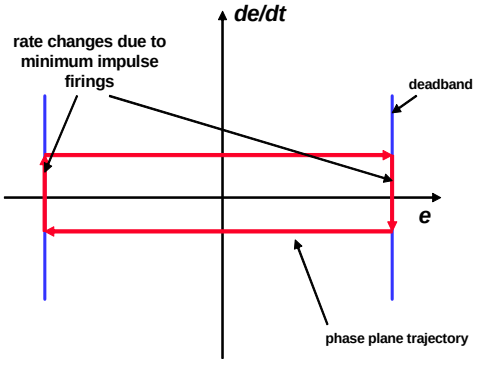

Figure 12. Two-sided Limit Cycle in Phase Plane

As mentioned above, control precision requirements are often driven primarily by final approach and docking requirements since attitude and translation deadbands are typically

smallest for these operations. Minimum rotational and translational rate change increments may be directly compared to docking rate error requirements. However, docking position and attitude error requirements do not relate directly to thruster precision. For this reason, the metric used to assess position and attitude precision was the time between firings required to maintain a commanded attitude or position under the assumption that control will evolve to a two-sided limit cycle as shown in Figure 12. The figure is a phase plane diagram with error (position or attitude) on the horizontal axis and error rate (velocity or angular rate) on the vertical axis. The red trace is the phase plane trajectory for a limit cycle in which the phase point drifts horizontally until encountering a deadband (blue line) where a thruster firing is assumed to instantaneously change the rate by one minimum rate quanta. These rate changes are assumed to be centered about the horizontal axis, as this produces a minimum time (worst case) limit cycle.

The time between thruster firings is ½ the limit cycle period, which may be expressed as:

$$\tfrac{1}{2}T = \frac{2\theta_{DB}}{\tfrac{1}{2}\ddot{\theta}t_{\min}} = \frac{4\theta_{DB}}{\ddot{\theta}t_{\min}} \tag{1}$$

where T is the limit cycle period, θ_{DB} is the attitude (or position) deadband, $\ddot{\theta}$ is the current axis component of the acceleration for each thruster fired, and t_{min} is the minimum thruster on time. For the assessments below, the rotational deadband was assumed to be 0.5°, and the translation deadband was 0.05 ft.

H. Robustness and Efficiency

Analytical methods exist for ascertaining the controllability of a thruster configuration based on the acceleration matrix, *A*, described above in the simplex section (Ref. [XX]). A "quick check" for robustness may be conducted using these methods by removing thrusters from the original configuration and assessing the resulting acceleration matrix for controllability. However, experience has shown that these methods do not always provide insight into "real world" robustness, where we are concerned not only with controllability, but also that the thruster failed configuration has no control regions of very low efficiency. Therefore, assessing the robustness of an RCS configuration to thruster failures is tantamount to assessing the efficiency of each thruster failed configuration.

For this reason, robustness/efficiency tools have been developed to scan the six DOF space of rate change commands for the reference configuration, and all possible thruster sets with single or dual thruster failures. A useful subset of the six DOF space of possible commands, is the space of rotation-with-zero-translation commands and translation-with-zero rotation commands. Visualization tools have been developed to show the efficiency results graphically. These tools allow comparison between configurations for nominal efficiency and robustness to thruster failures. Quick look comparisons can also be made by simply using simplex for to determine the total on-time for all thrusters required to actuate the single-axis commands (X, Y, Z, roll, pitch, yaw). This total on-time is proportional to the propellant required for these commands and provides a good metric for comparing efficiencies. On-times were determined for the no-failure case and for single and dual thruster failures. In the failure cases, the on-time for the worst failed thruster or thruster combination was computed. These results were calculated for 25-lbf thrusters only since the 100-lbf results are simply ¼ of the 25-lbf numbers.

Recall that thruster on-time analysis relates propellant to rate changes. Efficiency is also related to control precision as discussed above. The firing rate analysis shown in the precision section above may be extended to provide a bounding estimate on fuel consumption for low disturbance environments. Given the limit cycle of figure 1, if *n* thrusters are fired at each deadband encounter, then the average propellant used over time is *n* times the minimum on time, times the flow rate of each thruster, divided by the firing period:

$$\dot{m}_{axis} = nt_{\min}\left(\frac{f}{I_{sp}}\right)\left(\frac{\ddot{\theta}t_{\min}}{4\theta_{DB}}\right) = \frac{nf\ddot{\theta}t_{\min}^2}{4I_{sp}\theta_{DB}} \tag{2}$$

Where $\dot{m}_{axis}$ is the average propellant used in a single axis, f is the single jet thrust (assumes all thrusts equal) and I_{sp} is the specific impulse of the jet at minimum on time.

Another useful form of (2) for attitude control approximates the per-axis angular acceleration as thruster force times an effective moment arm, *l* divided by the inertia in the associated axis:

.

$$\dot{m} = \left(\frac{nf^2 t_{\min}^2 l}{4 I_{sp} I_{xx} \theta_{DB}} \right)_{roll} + \left(\frac{nf^2 t_{\min}^2 l}{4 I_{sp} I_{yy} \theta_{DB}} \right)_{pitch} + \left(\frac{nf^2 t_{\min}^2 l}{4 I_{sp} I_{zz} \theta_{DB}} \right)_{yaw} \quad (3)$$

Where l is the "effective" moment arm and I_{xx}, I_{yy}, I_{zz} are the moments of inertia for each axis. This form clarifies the effects of thruster size and minimum on time for fuel consumption in a two-sided limit cycle. Note that propellant consumption is proportional to the square of thrust magnitude and minimum on time.

It should be noted that the expressions in (2) and (3) assume the worst-case, centered two sided limit cycle. This is bounding for a no-disturbance environment. However, when disturbances are significant, the "rate change" efficiency discussed above determines fuel consumption and a different approach must be taken to estimate average usage. These analytic estimates of prop consumption serve several purposes: they provide insight into how a particular configuration effects attitude hold performance, they provide initial propellant estimates for early tank sizing and other systems engineering activities, and they provide a check on simulation results.

I. Plume Impingement

One very important consideration for RCS sizing and layout was plume impingement, particularly on CEV solar arrays. In order to assess the relative merits of the six candidate configurations, a … COMPLETE WITH HELP FROM F. LUMPKIN

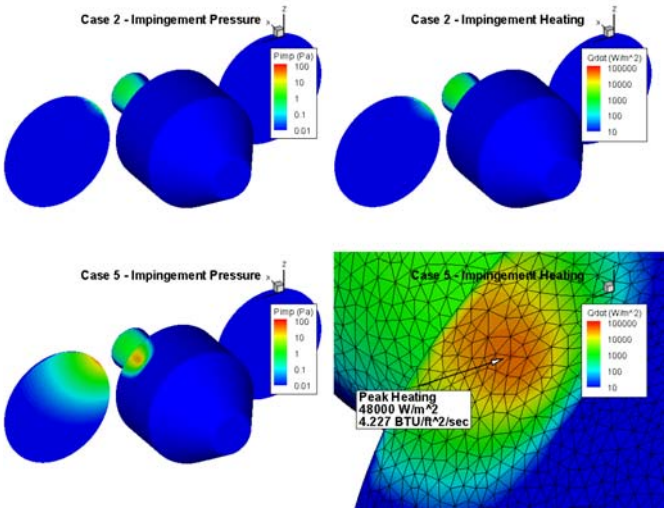

Figure 13. Example RCS Plume Impingement Analysis

VI. Simulation Assessment

This section describes the simulation algorithms used to assess candidate RCS configurations, and describes the scenarios used to evaluate RCS performance.

A. Reconfigurable Control Algorithm Description

The need to quickly assess multiple RCS configurations led to the development of a control design that is parameterized by thruster locations, directions and thrust magnitudes. This was achieved by using a proportional-derivative (PD) control law, coupled with a simplex thruster selection algorithm that also served to perform pulse width modulation (PWM) to approximate linear performance in some operating regions.

The rotation and translation control modules consist of PD control laws, simplex thruster selection and pulse width modulation logic (Figure 14).

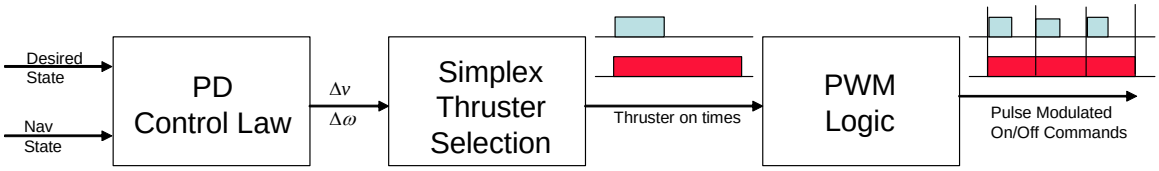

Figure 14. Control Overview

The PD control laws operate on position and velocity, or attitude and angular rate errors to generate rate change commands according to:

$$\Delta v = K_p x_{err} + K_v v_{err}$$
$$\Delta \omega = K_\theta \theta_{err} + K_\omega \omega_{err} \tag{4}$$

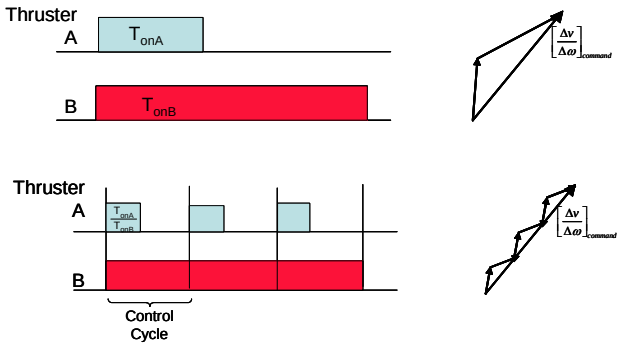

Figure 15. Pulse Modifications for Saturated Firings and Resultant Rate Change Profiles

Minimum values may be imposed via inputs on the Δv and $\Delta \omega$ commands. This allows the user to set effective deadbands by setting the control law gains and command minima as discussed below.

The Δv and $\Delta \omega$ commands are processed by the simplex thruster selection logic as described above. The net effect of the simplex thruster selection is to generate thruster on times commands for all thrusters (for 6DOF control, no more than 6 will be non-zero). These on-time commands are a form of pulse-width modulation with larger rate changes requiring longer on-times. The control law approximates a linear system as long as the commands do not cause on-times that exceed the discrete system time step – 1 second in the ANTARES simulation.

For on-time commands less than 1 second, the PWM logic passes the unmodified commands to the RCS model where they are quantized and actuated. When the maximum on-time command is greater than 1 second, the control system is saturated. In this case, the PWM logic normalizes all on-times by the maximum on-time. This causes the thruster with the longest on-time to fire for the entire control cycle, while thrusters with shorter on-times fire for a percentage of the control cycle. Figure 15 shows an example for a two-thruster command. This scaling has the effect of "spreading out" shorter thruster firings across the overall firing duration – causing the actuated rate change to remain nearer the commanded rate change as shown in the figure.

For the purposes of achieving desired attitude or position accuracy, it is useful to view the PD control law as a set of regions in the phase plane. Figure 16 depicts the switch limits that arise from the control law, thruster quantization, and pulse width modulation. These switch curves determine effective deadbands in position (or attitude) and velocity (or angular rate). If desired, control gains may be used to achieve a desired time response, or to set effective deadbands, or both.

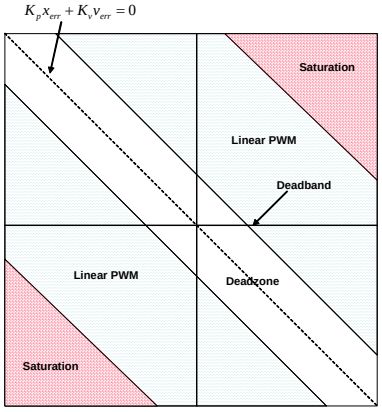

Figure 16. PD Control Correspondence to Phase Plane

B. Simulation Analysis Description: Proximity Operations and Docking

6-DOF simulation assessments of each configuration were conducted using the ANTARES [] simulation. The purpose of the simulation analysis was to generate comparative propellant consumption rates for a critical portion of the flight and to confirm required control performance for each configuration in a representative scenario. To this end, a proximity operations and docking scenario was generated that included translation maneuvers, attitude control and pointing, and 6-DOF control during the final approach.

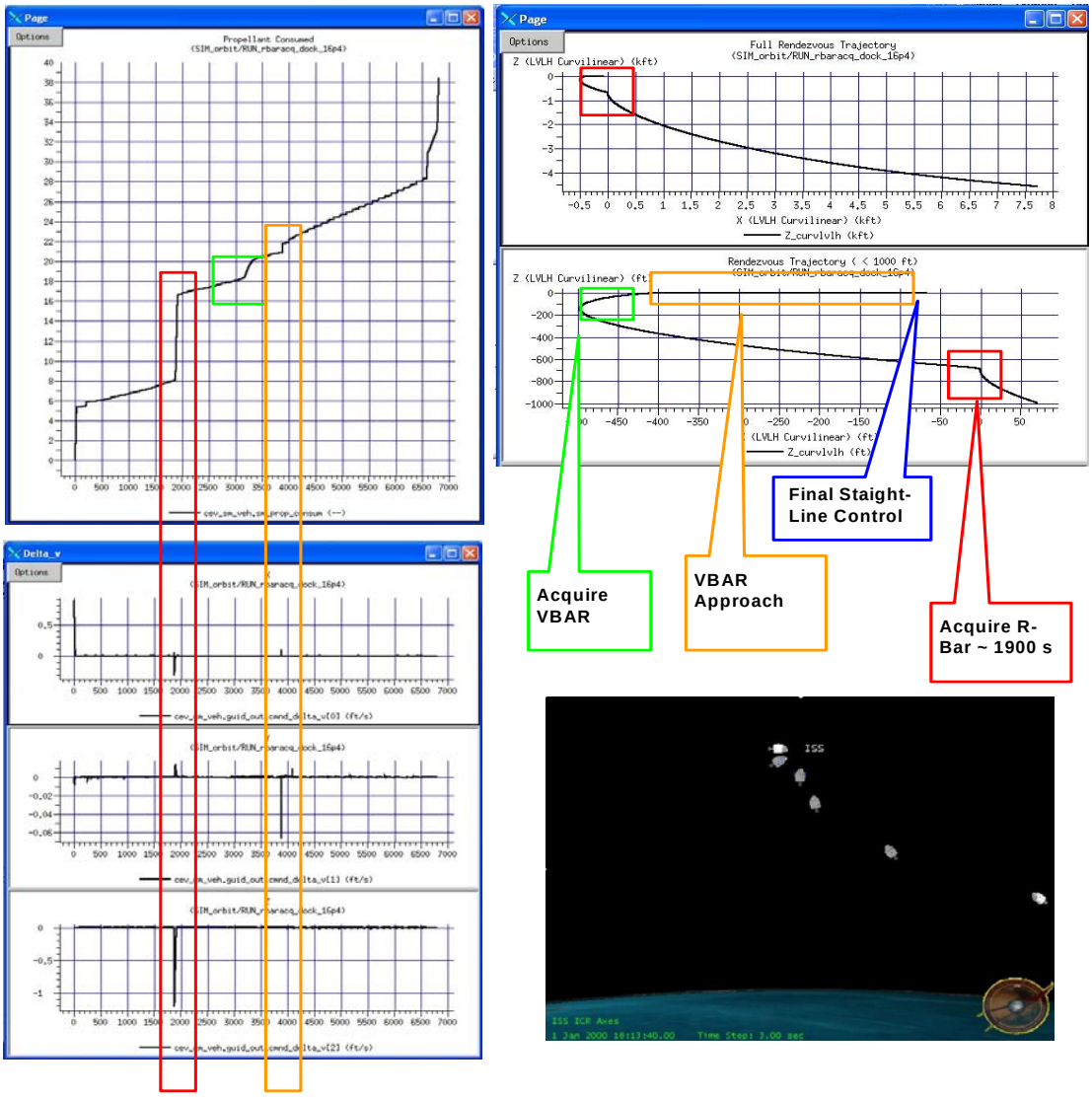

Figure 17. Proximity Operations Trajectory Example

The simulation was configured to use perfect sensor/navigation modeling with Rendezvous and Proximity Operations Program guidance [] used throughout most of the trajectory until final approach when straight line guidance was used for docking. Figure 17 shows some example plots and visualizations of the trajectory. Fuel consumption is shown in the upper left plot, and the large steps in propellant use are correlated with the commanded velocity changes shown on the lower left plots. These velocity changes cause the vehicle to fly the trajectory shown in the upper right plots.

The relative trajectory plots show the in-plane path with the target vehicle velocity pointing left. The trajectory includes an Rbar acquisition phase (initial curve to Rbar), followed by a transition to Vbar (second curve from Rbar to Vbar), followed by a Vbar approach, and finally a final straight-line approach for the last few feet.

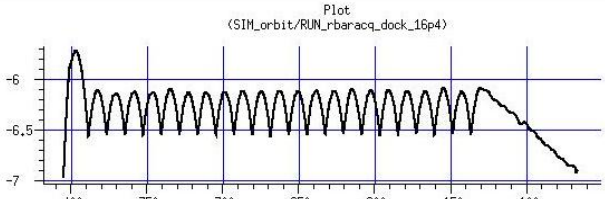

Figure 18. Final Vbar Approach

Throughout the trajectory, the CEV $+x_{body}$ axis points at the International Space Station (bottom right graphic). The roll orientation starts "windows down" and finishes "windows up" so that no roll maneuvers are required during the approach. Control gains are set to achieve a 0.5° deadband throughout the entire trajectory.

This scenario includes 3-DOF attitude hold/pointing control and two variations of 6-DOF RCS control: multiaxis burn control and 6-DOF feedback control. The multiaxis burn mode is used to actuate velocity change commands from guidance and tests the capability of the RCS configuration to maintain rotational control while actuating translation commands. This mode is used to effect the initial burn to place the CEV on a coasting trajectory to Rbar, the burn to depart the Rbar and coast to Vbar, and the burn to acquire Vbar. Additionally, this mode is used through most of the final approach to move along the Vbar in a series of fuel efficient hops (Figure 18).

The 6-DOF feedback control mode is used during the final approach. This mode tests the ability of the RCS configuration to maintain fine attitude and translation control simultaneously.

C. Simulation Analysis Description: Low Lunar Orbit Attitude Hold

The ANTARES simulation was also configured to perform attitude hold performance testing. The simulation was configured in Lunar orbit at various initial attitudes. Twenty six simulations were conducted at each of several LVLH attitudes with initial rate errors evenly distributed over the sphere of possible rate errors. LVLH attitude holds were performed for 25000 seconds (about 7 hours) each. 15 degree deadbands were used. Some example performance from these runs are provided in the results section below in the efficiency discussion.

VII. Results

This section contains example results for each of the major metrics for all configurations and summarizes them to explain the decisions made.

A. Authority

Table 2 shows the instantaneous translation authority results for each of the configurations. These are normalized by the authority requirements, so numbers greater than 1.0 are desired. The requirements were derived from desired closure and backout acceleration as well as the need to counter apparent disturbances in the LVLH coordinate system. Configurations meeting the requirements are in green, near or below the requirement are in yellow. Note that positive x_{body} control authority is high for all configurations since those configurations with smaller thrusters have augmented axial thrusters. The effects of thruster cant can be seen in the comparison of lateral control authority between configurations 1 and 2. Note that configurations 4 and 5 were slightly below the requirement for axial acceleration in $-x_{body}$ due to smaller, 14 lbf thrusters canted at 45 degrees in the Modified Block Swap Geometry.

Table 2. Instantaneous Control Authority Normalized by Requirement

Direction	Config 0	Config 1	Config 2	Config 3	Config 4	Config 5	Config 6
+X	3.6	3.6	3.6	16.3	6.8	4.7	4.7
-X	9.1	9.1	9.1	3.3	0.9	0.9	5.0
Lateral	6.7	6.7	2.1	1.7	1.2	1.2	1.5

Figure 19. compares the average translational accelerations for configurations X and X. Note that the aft pod mounting of configuration X results in significantly lower average lateral control acceleration when modulation due to rotational control is accounted for.

INSERT FIGURE 19 WITH SPHERE OF AVERAGE CONTROL ACCELS

Not surprisingly, the larger thruster configurations had more control authority. It was also noted that the aft pod mounted schemes paid more of a penalty in average authority than pods mounted near the center of mass.

B. Precision

Table 3 has the rotational precision results by configuration. These results were derived from the minimum angular rate change afforded in the worst (largest rate change) axis. Again the results are normalized by the

requirement – but since smaller incremental rate changes are desirable, numbers less than 1.0 are in green. Here, we have shaded the precision value that exceeded 15% of the requirement. Recall that for docking precision, the 100 lbf configurations (0, 1 and 2) were allowed 20 ms minimum on-time. Concentrating for the moment on the Roll precision results, note that configurations 1 and 3 are nearly identical. Configuration 1 used 100 lbf thrusters at 20 ms, and configuration 3 used 25 lbf at 80 ms, so it is not surprising that minimum rate changes were nearly the same (slight mounting differences account for the variance). This underscores the fact that precision is largely a function of thruster size and minimum allowable on time. However, one exception to this rule is configuration 2, whose roll authority is greatly reduced by the small cant angle in the MBSG layout.

Table 3. Control Precision Normalized by Requirement

Direction	Config 0	Config 1	Config 2	Config 3	Config 4	Config 5	Config 6
Roll (d/s)	1.03	1.17	0.04	1.15	0.22	0.22	0.40
Pitch (d/s)	0.97	1.14	1.07	0.71	0.39	0.39	0.70
Yaw (d/s)	0.98	0.72	0.84	0.45	0.37	0.37	0.67

Even with 20 ms minimum on time allowed, none of the 100 lbf configurations met the docking precision requirements – although the Baseline and configuration 2 were close. However, for long duration attitude hold, 80 ms was the minimum on time, and the next section shows the effect of the resulting larger minimum rate change on efficiency.

C. Efficiency

As discussed above, two measures of efficiency were considered: rate change efficiency, and long term attitude hold efficiency. Rate change efficiency was evaluated using the simplex thruster selection algorithm to find optimal thruster on times for translation and rotation rate change commands. For translation commands, rotation was commanded to zero, and vice versa.

Table 4. shows the rate change efficiency for rotational rate changes for each of the configurations.

INSERT RATE CHANGE EFFICIENCY TABLE 4

Long term attitude hold was evaluated in a Lunar LVLH hold scenario, where disturbances were assumed small. Equation (2) was used to find the centered, two-sided limit cycle usage for each of the configurations for a range of deadbands, assuming t_{min} = 80 ms. Thruster specific impulse was assumed to be 250 sec for all configurations. The results are shown in Figure 19. The figure highlights the effects of thruster magnitude for a given minimum on time. Note that all of the 100 lbf configurations (Baseline, 1, and 2) exhibited significantly higher usage rates than the other configurations. Also, the 25 lbf configurations lie between the 100 lb and 14 lb configurations, as expected. Selected results were confirmed with simulation runs. These are depicted by the asterisks at a particular deadband in the figure. Note that the simulation generally resulted in lower usage than the theoretical worst case, but that the trend in thruster magnitude holds.

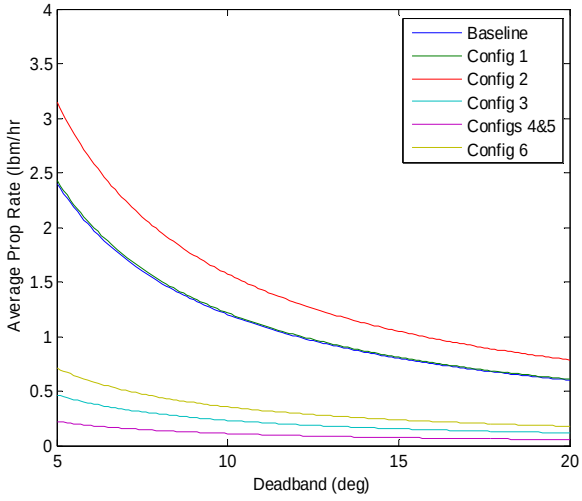

Figure 19. Propellant Usage by Deadband for Each Configuration

ADD SIMULATION RESULTS TO FIGURE

Figure 20 contrasts simulation results for two Lunar attitude holds. The left plots in each group are phase plane depictions of angular rate error versus attitude error, while the right plots depict the resulting control torques (each torque spike represents a firing at an attitude deadband). Note that the more centered limit cycles result in higher firing rates and more fuel consumption. This phenomenon accounts for most of the variance in the simulation results above. Note also that the simulation results are bounded by the worst case analytical curves.

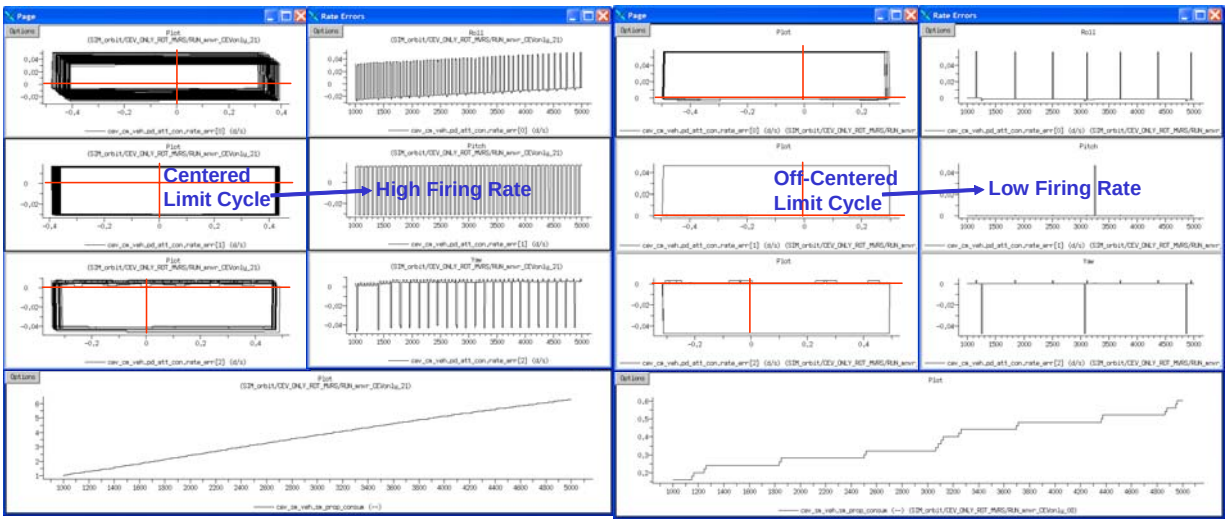

Figure 20. Simulation Results Depicting Centered and Off-Centered Limit Cycles

D. Robustness

The simplex-based robustness analysis described above was performed for each of the configurations. The efficiency metric used was the ratio of the propellant used to effect a rate change with no failures, divided by the propellant required with one or two failures. Table 4 collects the efficiency ratios for the worst command direction for the worst single or dual thruster failure for each of the configurations. Note that the Modified Block Swap Geometries (2,4,5 and 6) do not degrade much with up to two failures since they consist of nearly identical strings of thrusters. The Baseline and Modified Baseline Layouts (0, 1 and 2) became much less efficient in worst case conditions, but none of the configurations became uncontrollable. The color codes in the table are subjective, since technically all configurations meet two fault tolerant requirements. However, the increase in propellant consumption with failures for some configurations was considered a drawback.

Table 4. Efficiency Ratios for Worst Failures

	Config 0	Config 1	Config 2	Config 3	Config 4	Config 5	Config 6
trans 1 failure	1.6	1.0	1.1	1.1	1.0	1.0	1.0
rot 1 failure	1.0	1.0	1.1	1.0	1.1	1.1	1.1
trans 2 failure	2.5	4.1	1.0	1.9	1.1	1.1	1.1
rot 2 failure	3.6	6.1	1.3	2.8	1.3	1.3	1.3

E. Proximity Operations Performance

Figure 21 shows a portion of the simulated proximity operations trajectories and Figure 22 has the associated propellant performance for each configuration. All of the configurations successfully docked. However, configurations 4 and 5, with 14 lbf thrusters in the MBSG, took longer to dock due to overshoots of the station keeping point at the beginning of the V-bar approach. Although this performance could probably be improved, the behavior highlights the low control authority of these 14 lbf configurations. Configuration 5 had a particularly large overshoot on arrival at V-bar since it not only used the smaller thrusters, but also had the aft-mounted pod scheme, which reduced effective lateral authority as discussed above.

Propellant usage tended to be dominated by translational maneuvers which are indicated by the large “jumps” in propellant in Figure 22. Because of this, thruster layouts which had good efficiency in translation tended to fare better. The poorest performance came from configuration 1, which used the Modified Block Swap Geometry, but with only a 15° cant (refer to Figure 11). The most efficient layout from the point of view of proximity operations was the Modified Baseline which was used by configurations 1 and 3. However, performance of the MBSG configurations was acceptable with 25 lbf thrusters or larger.

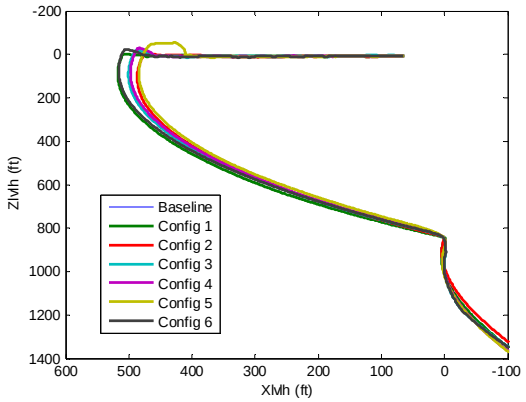

Figure 21. RBAR to Docking Trajectories for Each Configuration

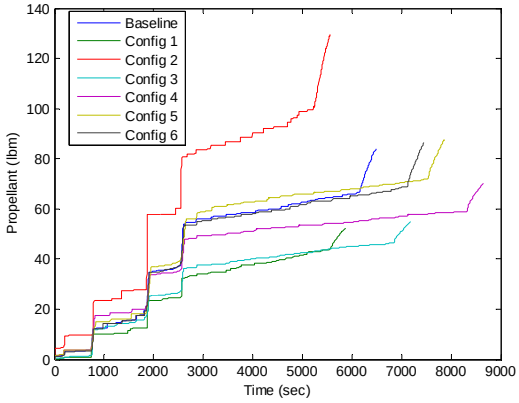

Figure 22. Propellant Use for Each Configuration

F. Summary

Table 5 summarizes the result discussed above. Green indicates acceptable performance, yellow indicates that performance was of concern or within 10% of the requirement, red indicates requirements not met. From this analysis, it became clear that many of the attributes of configuration 6 were desirable. These included 25 lbf thrusters with augmented axial engines providing good precision and acceptable authority, and the Modified Block Swap Geometry for robustness. However, it was concluded that placing the thrusters further forward could improve effective translation authority and efficiency, so the recommended configuration for the next baseline was configuration 6 with thruster pods mounted in the forward location.

Metric	Baseline (Config 0)	Config 1	Config 2	Config 3	Config 4	Config 5	Config 6
Translational Authority							
Rotational Precision							
Proximity Operations							
Efficiency							
Robustness							

VIII. Conclusion

This paper has provided an overview of the tools and techniques used to assess candidate RCS configurations for control of the CEV. Off line analysis included assessments of precision, authority, robustness and efficiency using simplex-based thruster selection algorithms and limit cycle analysis. Time domain simulation tools also used simplex thruster selection and pulse width modulation control laws to facilitate rapid assessment of multiple configurations.

Seven total RCS configurations were assessed including a baseline configuration and six candidate configurations. A unique thruster layout – the Block Swap Geometry – was evaluated and found to provide good robustness and acceptable performance in other areas. Attributes from the trade space were selected to form the final configuration, which included a Modified Block Swap layout, 25 lbf thrusters, and additional augmentation thrusters. This configuration provides robust performance and good precision with the stipulated minimum on time.

Acknowledgments

The Authors wish to acknowledge …

Ed McCants, Rich Burt, Adrian Adamson (BSG guy). Forrest Lumpkin etc.

References